Journal of the Serbian Chemical Society
JSCS-info@shd.org.rs • www.shd.org.rs/JSCS
J. Serb. Chem. Soc. *86* (11) 1075–1087 (2021)
JSCS–5484
Original scientific paper
Published 14 September 2021

Electrodeposition of aluminum-doped thin silicon films from a KF–KCl–KI–K_2SiF_6–AlF_3 melt

MICHAEL V. LAPTEV, ANASTASIA O. KHUDOROZHKOVA, ANDREY V. ISAKOV*, OLGA V. GRISHENKOVA, SERGEY I. ZHUK and YURII P. ZAIKOV

Ural Branch of the Russian Academy of Sciences, Institute of High Temperature Electrochemistry, 20 Academicheskaya St., 620137 Ekaterinburg, Russian Federation

(Received 17 September 2020, revised 16 August, accepted 17 August 2021)

Abstract: The regularities of silicon and aluminum co-deposition on glassy carbon from KF–KCl (2:1)–75 mol % KI–0.15 mol % K_2SiF_6–(up to 0.15 mol %) AlF_3 melts at 998 K were studied by cyclic voltammetry, chronoamperometry, scanning electron microscopy, atomic force microscopy and Raman spectroscopy. The cyclic voltammograms demonstrated the presence of only one cathodic peak (or nucleation loop at a low reverse potential) and the corresponding anodic peak. The cathodic peak shifted in the cathodic direction with decreasing concentration of aluminum ions in the melt or with increasing scan rate. The Scharifker–Hills model was used to analyze potentiostatic current density transients and estimate the values of the apparent diffusion coefficient and the number density of nuclei. The morphology and elemental analysis of the samples obtained during potentiostatic and galvanostatic deposition for 30–60 s were studied. Continuous thin silicon films doped with aluminum were obtained under galvanostatic conditions.

Keywords: molten salts; co-deposition; kinetics; 3D nucleation/growth.

INTRODUCTION

Silicon is the dominant source material for the production of electronic devices, solar cells and anode materials for Li-ion batteries (LIBs) because it is an intrinsic semiconductor and has excellent physicochemical properties and stability.[1,2] The use of thin Si films improves the characteristics of photovoltaic devices and advanced LIBs. In particular, thin-film silicon solar cells compensate for many of the disadvantages of conventional ones and expand the range of applications.[2,3] Thin Si films improve cycle stability and rate capabilities of the batteries and retain the structural integrity of the anodes during operation.[4]

* Corresponding author. E-mail: ihte_uran@mail.ru
https://doi.org/10.2298/JSC200917065L

There are various ways for producing thin Si films, *e.g*. plasma-enhanced chemical vapor deposition (PECVD) and liquid phase crystallization (LPC) are widespread.[5–8] Electrodeposition from molten salts is a promising method for producing thin silicon films due to the simplicity of the process, and the low capital and operating costs.[9–19] In addition, high deposition rates of continuous silicon layers and the ability to control the structure and morphology of films are the advantages of this technique.

Suitable process media are silicon-containing melts based on alkali metal halides. In particular, the molten KF–KCl–K_2SiF_6 mixture is a good electrolyte for obtaining continuous Si films.[10,14–18] Stability in the silicon concentration, relatively low operating temperatures (from 923 K), solubility in water, and less aggressiveness in comparison with pure fluoride melts are important advantages of this electrolyte. Partial replacement of KF–KCl with potassium iodide contributes to an additional decrease in the aggressiveness of the melt and the liquidus temperature. In addition, a decrease in the electrical conductivity of melts with KI provides for the formation of more compact deposits.[20–22] Thin (≈600 nm for 1-2 min) continuous silicon films with good adhesion are formed on glassy carbon and tungsten substrates during electrodeposition from a KF–KCl (2:1)––75 mol % KI–0.5 mol % K_2SiF_6 melt.[23]

Electrolytes based on KF–KCl–K_2SiF_6 and KF–KCl–KI–K_2SiF_6 can also be used to obtain doped silicon films by co-deposition of silicon with a selected dopant (*e.g*., P, B, Al). Apparently, this approach can be useful for the manufacture of silicon films (n-type, p-type and p–n junction) with various thicknesses and surface morphologies, which is important for the simplified production of photovoltaic and optoelectronic devices. For example, high-quality tin-doped silicon films with n-type semiconductor behavior (a photocurrent up to 44 % that of a commercial n-type Si wafer) from the KCl–KF–1 mol % K_2SiF_6 melt containing 0.020–0.035 wt. % Sn were electrodeposited.[18] Doping of silicon films with aluminum can facilitate the production of p-type silicon materials[19] that are promising for a number of applications in solar cells.[24,25]

To date, there are no published data on the co-deposition of silicon and aluminum from KF–KCl–K_2SiF_6 and KF–KCl–KI–K_2SiF_6 melts. Only information is available on the production of Al–Si alloys by electrolysis of cryolite melts with SiO_2 additives[26,27] and aluminum-doped silicon films (p-type) from a CaO––$CaCl_2$–SiO_2–Al_2O_3 melt.[19]

The aim of this work was to determine the regularities of the electrochemical co-deposition of silicon with aluminum on glassy carbon from KF–KCl (2:1)–75 mol % KI–K_2SiF_6–AlF_3 melts with different mole ratios of the depositing ions as well as to study the effect of electrodeposition conditions on the morphology and elemental composition of thin films.

EXPERIMENTAL

The starting materials for the preparation of the electrolyte were KF·HF (99.95 wt. %, Chimreaktivsnab, RF), KCl (99.98 wt. %, Chimreaktivsnab), K_2SiF_6 (99.92 wt. %, Vekton, RF), KI (99.9 wt. %, Vekton, RF) and AlF_3 (99.9 wt.%, Vekton, RF).

The electrolyte components were pretreated. A mixture of KF·HF and KCl powders was placed in a glassy carbon crucible and heated with the stepwise increase in temperature (2 h at 373 K, 3 h at 573 K) for thermal decomposition of KF·HF and removal of HF. Then the salts were melted and exposed at 1023 K for 2 h. Potassium iodide was purified from oxygen-containing impurities by heating a mixture of KI with an excess of crystalline iodine in the same way as in:[28]

$$2K_2O + 2I_2 \rightarrow 4KI + O_2\uparrow \quad (1)$$

The process was carried out at 723 K until evaporation of the iodine. Then KI was remelted and kept at 1073 K for 1 h. Potassium hexafluorosilicate was mixed with 2 wt. % NH_4F in a glassy carbon crucible and exposed to 673 K for 6 h to remove the oxygen-containing impurities:[29]

$$4NH_4F + SiO_2 \rightarrow 4NH_3\uparrow + SiF_4\uparrow + 2H_2O\uparrow. \quad (2)$$

A similar procedure was used to purify AlF_3. The prepared salts were stored in a dry box.

In this work, we used KF–KCl (2:1)–75 mol % KI–K_2SiF_6–AlF_3 melts with concentrations c_{Si} = 0.15 mol% and c_{Al} from 0.015 to 0.15 mol % were used. Before the experiment, the salts were mixed in the required amounts in a glassy carbon crucible, heated to 998 K, and held for 1 h. This melt was subjected to galvanostatic purification electrolysis at cathode current densities of 0.05 and 0.1 A·cm^{-2} (for 1 h and 20 min, respectively). The chemical composition of the electrolyte (before and after testing) was monitored by the atomic emission spectroscopy with inductively coupled plasma using iCAP 6300 Duo (Termo Scientific, USA).

The experiments were carried out in a three-electrode quartz cell (Fig. 1) in an atmosphere of high-purity dehydrated argon at 998 K. A nickel shield (2) protected the cell walls from interaction with sublimates.

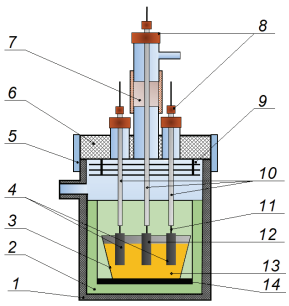

Fig. 1. Scheme of the experimental cell: 1 – quartz cell; 2 – Ni shield; 3 – glassy carbon crucible; 4 – Si electrodes; 5 – vacuum-rubber cuff; 6 – fluoroplastic cover; 7 – vacuum-rubber sluice device; 8 – rubber seals; 9 – Ni shields; 10 – quartz covers for current leads; 11 – tungsten current leads; 12 – working glassy carbon electrode; 13 – melt; 14 – graphite support.

A glassy carbon crucible (3) placed on a graphite support (14) served as a container for the electrolyte. Monocrystalline silicon plates (99.9999 wt. %) were used as a reference electrode and an auxiliary electrode (4), when performing electrochemical measurements) The working glassy carbon electrode (12) (SU-2000, Uralmetalgraphit, RF) was washed with distilled water, degreased with ethanol, and dried under vacuum. Tungsten rods (11) protected by quartz covers (10) served as current leads. A sluice device (7) was provided for replacing the working electrode during the experiment.

Cyclic voltammetry, chronoamperometry, and scanning electron microscopy with energy-dispersive X-ray spectroscopy (SEM-EDS) were used to study cathodic processes and the initial stages of electrocrystallization. The electrochemical measurements were performed using an Autolab PGStat302N with Nova 2.1.2 software. The resistance of the circuit was determined by the FRA method before each series of measurements and compensated using Autolab.

Al-doped thin Si films were obtained under galvanostatic and potentiostatic conditions. The samples were washed in boiling distilled water for 10–15 min to remove electrolyte residues. A Tescan Mira 3 LMU scanning electron microscope (Tescan, CR) equipped with an energy-dispersive X-ray spectrometer. Oxford instruments INCA Energy 350/X-max 80 was used to study the morphology and elemental analysis of deposits. A number of samples were additionally examined using a Bruker Dimension FastScan atomic force microscope (Bruker, Germany) with the ScanAsyst system.

The Raman spectra of samples were recorded using a Raman microscope-spectrometer Renishaw U1000 (Renishaw, UK) with confocal Leica DML microscope (50×, 100× objective, a notch filter, and a cooled charge-coupled device (CCD) detector) at the excitation of spectra by argon laser (the wave length 514.5 cm^{-1}, power of 20 mV) in the range of 50-1900 cm^{-1} and exposure time of 30–120 s. The spectral resolution was ±2 cm^{-1}, and wave number accuracy was about ±1 cm^{-1}; the laser beam had a focal-spot ≈1 μm in diameter.

RESULTS AND DISCUSSION

A typical series of cyclic voltammograms (CVs) obtained in the KF–KCl (2:1)–75 mol % KI–0.15 mol % K_2SiF_6–0.03 mol % AlF_3 melt (mole ratio $\gamma = c_{Si}/c_{Al} = 5$) at scan rates ($\nu$) from 0.1 to 1.5 $V \cdot s^{-1}$ are presented in Fig. 2a. It can be seen that the CVs are characterized by the presence of a single cathodic peak and the corresponding anodic peak. It should be noted that the shape of CVs is similar to that observed in the KF-KCl (2:1)–75 mol % KI–K_2SiF_6 melt, which does not contain aluminum ions.[23] Apparently, the presence of only one cathodic peak indicates a single-stage discharge of Si (IV) and Al (III) (*i.e.*, Si(IV) + 4*e* = Si and Al(III) + 3*e* = Al) and similar values of their electroreduction potentials under these conditions. The nucleation loop characteristic of the stage of nucleateon/growth on a foreign substrate[30–32] was detected in the cathode region when the reversal point was lower than the potential corresponding to the cathodic peak, $|E_\lambda| < |E_p|$ (Fig. 2b).

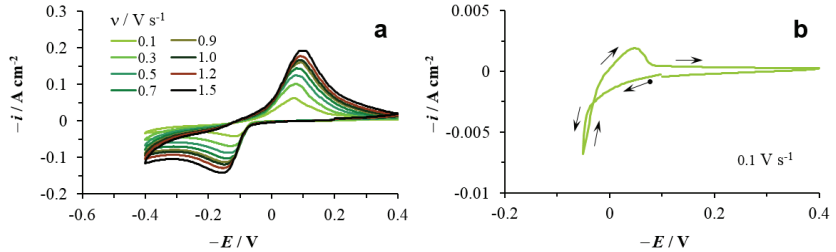

Fig. 2. Typical series of cyclic voltammograms (a) and a nucleation loop (b) obtained in the KF–KCl (2:1)–75 mol % KI–0.15 mol % K_2SiF_6–0.03 mol % AlF_3 melt ($\gamma = c_{Si}/c_{Al} = 5$) on glassy carbon at 998 K. The scan rate values are given in the figure. In this work, cathode currents and potentials were considered to have positive values (for convenience of calculations and discussion).

The same regularities were observed in melts with mole ratio $\gamma = 10$ and $\gamma = 1$ (Fig. 3). A comparison of CVs in melts with different concentrations of aluminum ions shows that E_p shifts in the anodic direction with increasing c_{Al} (Fig. 3a, c). In all cases, the cathodic peaks shifted in the cathodic direction with increasing scan rate, which indicates the quasi-reversibility or irreversibility of the process under these conditions. Figs. 3b, c demonstrate that at $\nu > 0.9$ V·s^{-1}, the electroreduction mechanism can be characterized as irreversible.

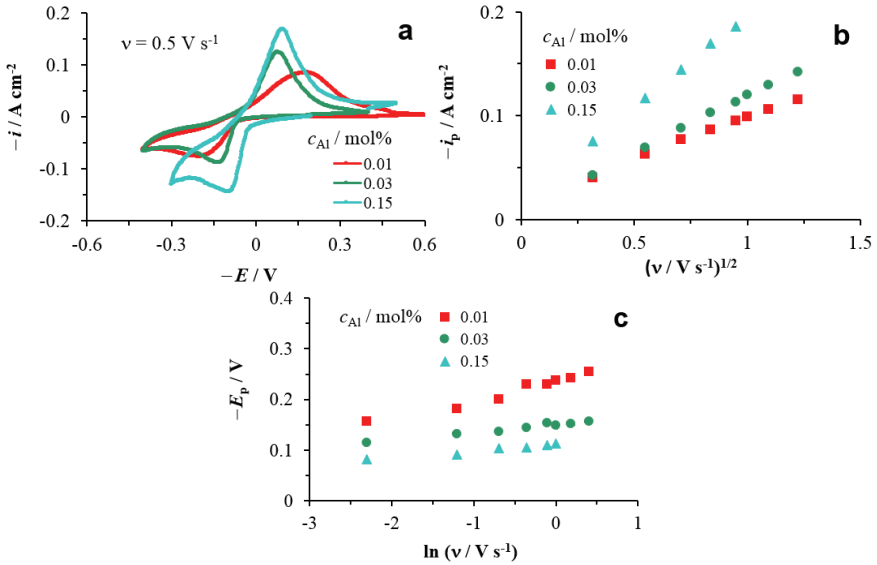

Fig. 3. Comparison of CVs (a), dependences of the cathode current density peak on the square root of the scan rate (b), and the dependences of the cathode peak potential on the logarithm of the scan rate (c) in KF–KCl (2:1)–75 mol % KI–0.15 mol % K_2SiF_6–AlF_3 melts with different concentrations of aluminum ions.

Typical families of potentiostatic current density transients, $i(t)$, obtained at co-deposition of silicon and aluminum from the melts with $\gamma = 1$ and $\gamma = 5$, respectively, are shown Figs. 4a and 5a. The form of these dependencies does not differ from the usual appearance for the electrocrystallization of silicon on glassy carbon.[14,20,23] Therefore, they could be qualitatively analyzed within the framework of the Scharifker–Hills model (SH model).[33,34] Fig. 4b demonstrates a comparison of experimental dependencies in the form of $(i/i_m)^2$ *vs.* (t/t_m) with dimensionless theoretical dependencies of the SH model for instantaneous and progressive nucleation with diffusion-controlled growth, respectively:

$$\left(\frac{i}{i_m}\right)^2 = \frac{1.9542}{t/t_m}\left\{1-\exp\left[-1.2564\left(t/t_m\right)\right]\right\}^2 \quad (3)$$

$$\left(\frac{i}{i_{\mathrm{m}}}\right)^2 = \frac{1.2254}{t/t_{\mathrm{m}}}\left\{1-\exp\left[-2.3367\left(t/t_{\mathrm{m}}\right)^2\right]\right\}^2 \quad (4)$$

where t_{m}, i_{m} are the coordinates of the maximum of $i(t)$.

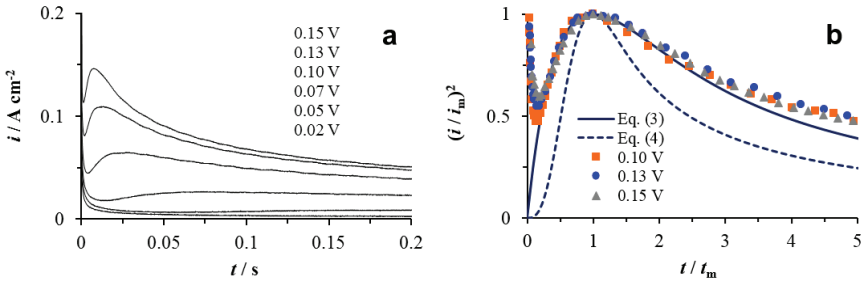

Fig. 4. Typical family of potentiostatic current density transients for co-deposition of silicon and aluminum from the KF–KCl (2:1)–75 mol % KI–0.15 mol % K_2SiF_6–0.15 mol % AlF_3 melt (a) and comparison of the experimental and theoretical (SH model) dimensionless dependences (b).

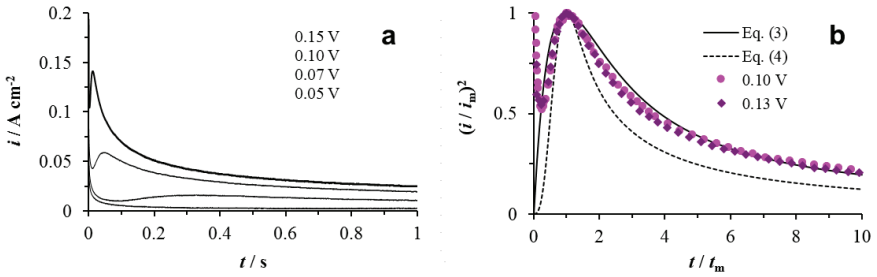

Fig. 5. Typical family of potentiostatic current density transients for the co-deposition of silicon and aluminum from the KF–KCl (2:1)–75 mol % KI–0.15 mol % K_2SiF_6–0.03 mol % AlF_3 melt (a) and comparison of experimental and theoretical (SH model) dimensionless dependences (b).

It can be seen that at $t/t_{\mathrm{m}} < 3$, the experimental dependences agree with the theoretical curve for instantaneous nucleation.

An approximate quantitative analysis is possible in this case under certain assumptions.[35,36] It was shown[36] that the equations of the SH model with modified values of the parameters can be used to estimate the apparent diffusion coefficient ($\tilde{D}$) and the number density of active centers (or nuclei in the case of instantaneous nucleation) on the electrode surface (N_0). Considering the total flux of two types of depositing ions in the electrolyte bulk and averaging the concentration profile with allowance for the mole ratio of the components (γ), gives for instantaneous nucleation:

$$t_{\mathrm{m}} = 1.2564/\pi\tilde{k}N_0\tilde{D} \quad (5)$$

$$i_{\mathrm{m}}{}^2 t_{\mathrm{m}} = 0.1629(\tilde{z}ec_0)^2\tilde{D} \quad (6)$$

$$\tilde{k} = (8\pi c_0 \tilde{\upsilon})^{1/2}\,,\ \tilde{\upsilon} = (\gamma \upsilon_{Si} + \upsilon_{Al})/(\gamma+1)\,,\ \tilde{z} = (\gamma z_{Si} + z_{Al})/(\gamma+1)$$

where c_0 is the bulk concentration of silicon ions, υ_{Si} and υ_{Al} are the volumes of Si and Al atoms, respectively (the volume of the new phase is the sum of the volumes of the individual components taking into account γ), z_{Si} and z_{Al} are the valances of the Si and Al ions, respectively.

Calculation with $\upsilon_{Si} = 2.01\times10^{-23}$ cm^3, $\upsilon_{Al} = 1.66\times10^{-23}$ cm^3, $z_{Si} = 4$, $z_{Al} = 3$, and $\gamma = 1$ gives $\tilde{z} = 3.5$, $\tilde{\upsilon} = 1.84\times10^{-23}$ cm^3, and $\tilde{k} = 8.31\times10^{-2}$. Substituting these values and $c_0 = 1.50\times10^{19}$ cm^{-3} into Eqs. (5) and (6), $\tilde{D}$ = = 1.43×10^{-5} cm^2 s^{-1} and $N_0 = 4.44\times10^7$ cm^{-2} were obtained for the curve at E = = 0.15 V.

Discrepancies with the theoretical dependence at $t/t_m > 3$ (Fig. 4b) should disappear at a lower concentration of deposited ions. In fact, this behavior can be observed in a melt with $\gamma = 5$ (Fig. 5b). In this case, the last portions of the current density transients coincide with the curve described by the Cottrell equation:

$$i = \tilde{z} e c_0 (\tilde{D}/\pi t)^{1/2} \qquad (7)$$

The $\tilde{D}$ value found from Eq. (7) was 1.38×10^{-5} cm^2 s^{-1}. This value is less than the diffusion coefficient of silicon ions in the KF–KCl (2:1)–75 mol % KI––0.5 mol % K_2SiF_6 melt, $D_{Si} \approx 1.95\times10^{-5}$ cm^2 s^{-1}.[23] This fact is consistent with more explicit diffusion limitations in melts with a higher concentration of aluminum ions (see Fig. 3a, c). The reasons may be the lower mobility of aluminum ionic complexes in comparison with silicon ones and a change in the structure of the complexes.

It was also noted that a more complex time dependence of the number density of nuclei is observed for a melt with $\gamma = 5$ in the potential range from 0.10 to 0.13 V, $N = N_0[1–\exp(–At)]$, where A is the nucleation rate constant. This is evidenced by the deviations of the experimental dimensionless curves at $t/t_m <$ < 5 from the theoretical one described by Eq. (3) (Fig. 5b), as well as the SEM and AFM images of nuclei (Fig. 6). Elemental analysis (Table I) demonstrates the presence of silicon and aluminum in the deposit composition; the availability of other components is due to the existence of electrolyte residues and oxidation of the surface of the deposit in air.

The morphology of the deposit obtained in the melt with the same concentration of depositing ions at the cathodic potential of 0.45 V for 60 s and the SEM-EDS maps for Si and Al are shown in Fig. 7.

It can be seen that the distribution of aluminum is quite uniform, but the surface of the deposit is not smooth but porous. More compact deposits can be produced at a cathodic potential of 0.2 V (Fig. 8). Continuous aluminum-doped silicon films were obtained under galvanostatic conditions at cathode current

densities from 0.025 to 0.1 A·cm^{-2} for $t \geq 30$ s from aq. melt containing 0.015 mol % AlF_3 (Fig. 9, Table I).

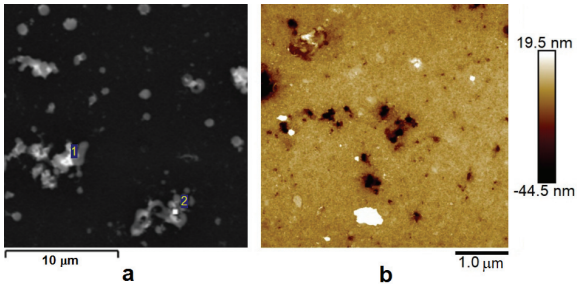

Fig. 6. SEM (a) and AFM (b) images of new-phase nuclei on glassy carbon during the co-deposition of silicon and aluminum from the KF–KCl (2:1)–75 mol % KI–0.15 mol % K_2SiF_6–0.03 mol % AlF_3 melt under potentiostatic conditions (E = 0.11 V, t = 0.04 s).

TABLE I. SEM-EDS data

Figure	Spectrum	Content, at. %						
		Si	Al	K	F	Cl	I	O
6a	1	13.61	0.90	11.28	0.49	1.17	7.04	65.51
	2	18.53	1.15	6.10	0.48	0.48	0.68	72.60
9d	1	85.42	0.34	2.59	0.56	–	–	11.09
	2	75.93	0.43	3.76	0.65	0.47	0.98	17.78
	3	87.09	0.44	2.97	0.61	–	–	8.890

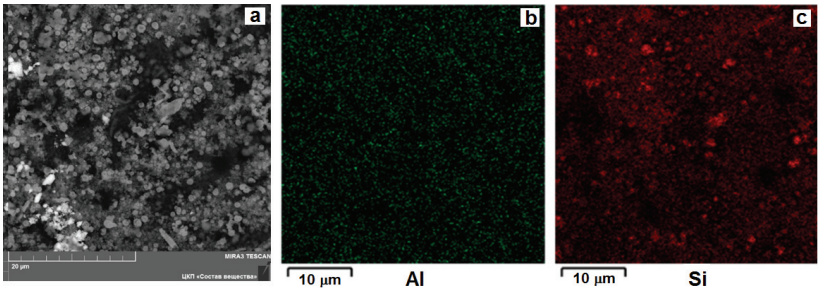

Fig. 7. SEM image of deposit (a) and maps of Al (b) and Si (c) after their co-deposition from the KF–KCl (2:1)–75 mol % KI–0.15 mol % K_2SiF_6–0.03 mol% AlF_3 melt under potentiostatic conditions (E = 0.45 V, t = 60 s).

A typical Raman spectrum of the Al-doped Si film on glassy carbon is shown in Fig. 10. The strong first-order Raman peak with a maximum at 511 cm^{-1} and two second-order bands at 300 and 940–1000 cm^{-1} can be attributed to the silicon vibrations.[17,37] In the high-frequency range, the spectrum contains two characteristic peaks at about 1330 and 1580 cm^{-1}, which correspond to the main carbon bands.[38] In general, this pattern is similar to the Raman spectrum of a continuous Si coating on C obtained in an earlier work.[17] The main differences are in

the shift of the strong band from the typical value for bulk crystalline Si (519 cm^{-1}) to 511 cm^{-1} and the expansion of its left flank towards the value typical for amorphous Si (480 cm^{-1}).[39] The same was observed in the Raman spectra of the Al-doped Si films obtained by radio-frequency magnetron sputtering, which did not have a well-crystallized structure.[39] Due to the fact that the atomic weights of Al and Si differ from each other by less than 4 %, the local mode produced by the additional Al atoms is very close to the strong Raman peak of Si and is difficult to identify even at a high Al concentrations.[40]

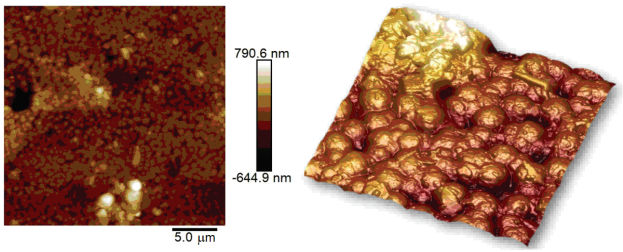

Fig. 8. AFM images of the deposit obtained from a KF–KCl (2:1)–75 mol % KI–0.15 mol % K_2SiF_6–0.03 mol% AlF_3 melt under potentiostatic conditions (E = 0.2 V, t = 30 s).

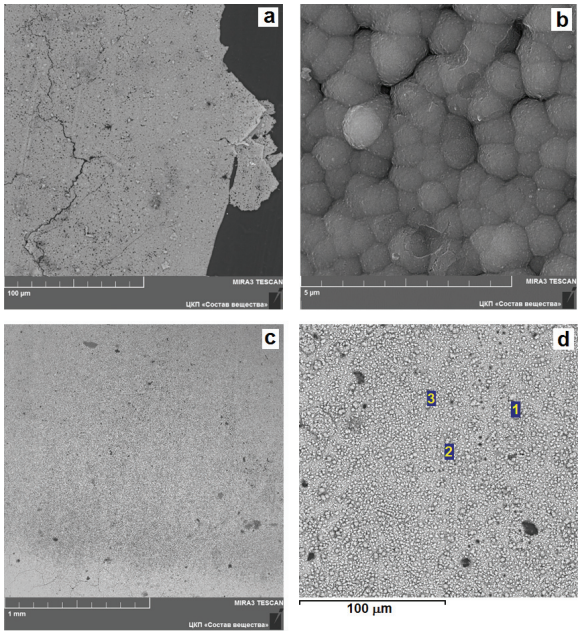

Fig. 9. SEM images of deposits obtained by co-deposition of silicon and aluminum from the KF–KCl (2:1)–75 mol% KI–0.15 mol % K_2SiF_6–0.015 mol % AlF_3 melt under galvanostatic conditions at 0.025 $A \cdot cm^{-2}$ (a, b) and 0.1 $A \cdot cm^{-2}$ (c, d) for 30 s. SEM-EDS data for Fig. 9d are given in Table I.

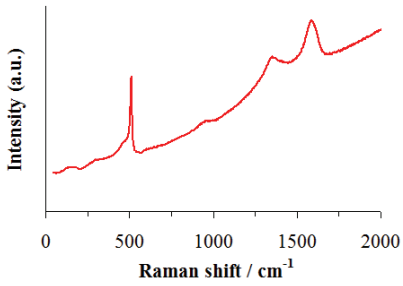

Fig. 10. Raman spectrum of an Al-doped Si film on glassy carbon. The electrodeposition conditions are the same as for Fig. 8.

CONCLUSIONS

The co-deposition of silicon and aluminum on glassy carbon from melts based on KF–KCl (2:1)–75 mol % KI containing 0.15 mol. % K_2SiF_6 and 0.015, 0.03, or 0.15 mol % AlF_3 at 998 K was studied. Analysis of cyclic voltammograms showed that: *i*) discharge of Si (IV) and Al (III) is a one-stage process; *ii*) the cathodic process can be characterized as quasi-reversible at scan rates from 0.1 to 0.9 $V \cdot s^{-1}$; *iii*) the share of diffusion limitations increases with increasing concentration of aluminum ions in the melt. The nucleation loop in the cyclic voltammograms at low reverse potentials and the shape of the potentiostatic current density transients indicate the presence of a 3D nucleation/growth stage. A comparison of dimensionless experimental and theoretical (the Scharifker–Hills model) dependencies demonstrated that instantaneous nucleation with the diffusion-controlled growth occurs in the melt with a mole ratio of Si and Al ion concentrations $\gamma = 1$. The nuclei appear gradually during electrodeposition from the melt with $\gamma = 5$. The apparent diffusion coefficient was estimated from the maximum of the current density transient (at $\gamma = 1$) and by the Cottrell equation (at $\gamma = 5$); its value was $\approx 1.4 \times 10^{-5}$ cm^2 s^{-1}. Analysis of the SEM-EDS and AFM data showed that continuous thin films of aluminum-doped silicon can be obtained under galvanostatic conditions at cathode current densities from 0.025 to 0.1 A cm^{-2}. Raman spectroscopy data indicate the formation of an amorphous phase.

Acknowledgements. The study is supported by the Russian Science Foundation Grant (project No. 16-13-00061). This work has been (partly) realized using the facilities of the shared access centers “Composition of compounds” (IHTE, UB RAS). The authors are grateful to ZEISS Russia & CIS (Moscow) for the demonstration measurements performed with a Bruker Dimension FastScan atomic force microscope.

ИЗВОД

ЕЛЕКТРОХЕМИЈСКО ТАЛОЖЕЊЕ ТАНКИХ ФИЛМОВА СИЛИЦИЈУМА ДОПИРАНИХ АЛУМИНИЈУМОМ ИЗ РАСТОПА KF–KCl–KI–K_2SiF_6–ALF_3

MICHAEL V. LAPTEV, ANASTASIA O. KHUDOROZHKOVA, ANDREY V. ISAKOV, OLGA V. GRISHENKOVA, SERGEY I. ZHUK и YURII P. ZAIKOV

Ural Branch of the Russian Academy of Sciences, Institute of High Temperature Electrochemistry, 20 Academicheskaya St., 620137 Ekaterinburg, Russian Federation

Законитости истовременог таложења силицијума и алуминијума из растопа KF–KCl (2:1)–75 mol % KI–0,15 mol % K_2SiF_6–(до 0,15 mol %) AlF_3 на подлогу од стакластог угљеника испитиване су коришћењем цикличне волтаметрије, хроноамперометрије, скенирајуће електронске микроскопије, микроскопије атомских сила и Раманове спектроскопије. Циклични волтамограми су показали присуство само једног катодног пика (или петље нуклеације при ниском повратном потенцијалу) и одговарајућег анодног пика. Катодни пик се померао у катодном смеру при смањењу конентрације јона алуминијума у растопу, као и при повећању брзине линеарне промене потенцијала. Шарифкер-Хилсов модел је коришћен за анализу потенциостатских струјних транзијената и процену вредности привидних коефицијената дифузије и густине нуклеуса. Испитавани су и морфологија и елементални састав узорака таложених под потенциостатским и галваностатским условима током 30–60 s. Континуални танки филмови силицијума допирани алуминијумом су добијени под галваностатским условима.

(Примљено 17. септембра 2020, ревидирано 16 августа, прихваћено 17. августа 2021)

REFERENCES

1. Y. Sakanaka, T. Goto, *Electrochim. Acta* **164** (2015) 139 (http://dx.doi.org/10.1016/j.electacta.2014.12.159)
2. S. C. Bhatia, *Advanced Renewable Energy Systems*, Woodhead Publishing India Pvt. Ltd., New Delhi, 2014 (ISBN-13: 978-9380308432, ISBN-10: 9380308434)
3. S. G. Dorofeev, N. N. Kononov, V. M. Zverolovlev, K. V. Zinoviev, V. N. Sukhanov, N. M. Sukhanov, B. G. Gribov, *Semiconductors* **48** (2014) 360 (https://doi.org/10.1134/S1063782614030105)
4. D. Ma, Z. Cao, A. Hu, *Nano-Micro Lett*. **6** (2014) 347 (https://doi.org/10.1007/s40820-014-0008-2)
5. M. Rohde, M. Zelt, O. Gabriel, S. Neubert, S. Kirner, D. Severin, T. Stolley, B. Rau, B. Stannowski, R. Schlatmann, *Thin Solid Films* **558** (2014) 337 (https://doi.org/10.1016/j.tsf.2014.03.008)
6. E. Yu. Gusev, J. Y. Jityaeva, O. A. Ageev, *Mater. Phys. Mech.* **37** (2018) 67 (http://dx.doi.org/10.18720/MPM.3712018_9)
7. D. Amkreutz, J. Haschke, T. Häring, F. Ruske, B. Rech, *Sol. Energy Mater. Sol. Cells* **123** (2014) 13 (http://dx.doi.org/10.1016/j.solmat.2013.12.021)
8. J. Haschke, D. Amkreutz, L. Korte, F. Ruske, B. Rech, *Sol. Energy Mater. Sol. Cells* **128** (2014) 190 (http://dx.doi.org/10.1016/j.solmat.2014.04.035)
9. R. Boen, J. Bouteillon, *J. Appl. Electrochem*. **13** (1983) 277 (https://doi.org/10.1007/BF00941599)
10. D. B. Frolenko, Z. S. Martem'yanova, A. N. Baraboshkin, S. V. Plaksin, *Rasplavy* No.5 (1993) 42 (in Russian) (https://www.elibrary.ru/item.asp?id=12739574)

11. S. I. Zhuk, V. A. Isaev, O. V. Grishenkova, A. V. Isakov, A. P. Apisarov, Yu. P. Zaykov, *J. Serb. Chem. Soc*. **82** (2017) 51 (https://doi.org/10.2298/JSC160712109Z)
12. J. T. Moore, T. H. Wang, M. J. Heben, K. Douglas, T. F. Ciszek, in *Conference Record of the 26th IEEE Photovoltaic Specialists Conference*, 1997, Anaheim, CA, USA, IEEE, Anaheim, 1997, p. 775 (http://dx.doi.org/10.1109/PVSC.1997.654204)
13. O. Chemezov, A. Apisarov, A. Isakov, Yu. Zaikov, *EPD Congress 2012*, in *Proceedings of the TMS 2012 Annual Meeting & Exhibition*, 2012, Orlando, FL, USA, *Proceedings TMS 2012*, L. Zhang, J.A. Pomykala, A. Ciftja, Eds., Wiley, New York, 2012, p. 493 (https://doi.org/10.1002/9781118359341.ch58)
14. Yu. P. Zaykov, S. I. Zhuk, A. V. Isakov, O. V. Grishenkova, V. A. Isaev, *J. Solid State Electrochem*. **19** (2015) 1341 (https://doi.org/10.1007/s10008-014-2729-z)
15. K. Yasuda, K. Maeda, T. Nohira, R. Hagiwara, T. Homma, *J. Electrochem. Soc*. **163** (2016) D95 (https://doi.org/10.1149/2.0791603jes)
16. K. Maeda, K. Yasuda, T. Nohira, R. Hagiwara, T. Homma, *J. Electrochem. Soc*. **162** (2015) D444 (https://doi.org/10.1149/2.0441509jes)
17. S. I. Zhuk, A. V. Isakov, A. P. Apisarov, O. V. Grishenkova, V. A. Isaev, E. G. Vovkotrub, Yu. P. Zaykov, *J. Electrochem. Soc*. **164** (2017) H5135 (https://doi.org/10.1149/2.0171708jes)
18. J. Peng, H. Yin, J. Zhao, X. Yang, A. J. Bard, D. R. Sadoway, *Adv. Funct. Mater*. **28** (2017) 1703551 (https://doi.org/10.1002/adfm.201703551)
19. X. Zou, L. Ji, J. Ge, D. R. Sadoway, E. T. Yu, A. J. Bard, *Nat. Commun*. **10** (2019) 5772 (https://doi.org/10.1038/s41467-019-13065-w)
20. Yu. P. Zaykov, S. I. Zhuk, A. V. Isakov, O. V. Grishenkova, V. A. Isaev, *Rasplavy* No.5 (2016) 441 (in Russian) (https://www.elibrary.ru/item.asp?id=36286045)
21. A. P. Apisarov, A. A. Redkin, Yu. P. Zaikov, O. V. Chemezov, A. V. Isakov, *J. Chem. Eng. Data* **56** (2011) 4733 (https://doi.org/10.1021/je200717n)
22. A. Khudorozhkova, A. Isakov, A. Apisarov, A. Redkin, Y. Zaikov, *J. Chem. Eng. Data* **65** (2020) 2505 (https://doi.org/10.1021/acs.jced.9b01161)
23. M. V. Laptev, A. V. Isakov, O. V. Grishenkova, A. S. Vorob'ev, A. O. Khudorozhkova, L. A. Akashev, Yu. P. Zaikov, *J. Electrochem. Soc.* **167** (2020) 042506 (https://doi.org/10.1149/1945-7111/ab7aec)
24. M. Rüdiger, M. Rauer, C. Schmiga, M. Hermle, S. W. Glunz, *Energy Procedia* **8** (2011) 527 (https://doi.org/10.1016/j.egypro.2011.06.177)
25. C. Gong, S. Singh, J. Robbelein, N. Posthuma, E. Van Kerschaver, J. Poortmans, R. Mertens, *Prog. Photovoltaics* **19** (2010) 781 (https://doi.org/10.1002/pip.1035)
26. P. S. Pershin, A. V. Suzdaltsev, Y. P. Zaikov, *J. Electrochem. Soc*. **163** (2016) D167 (https://doi.org/10.1149/2.0521605jes)
27. A. Liu, Z. Shi, X. Hu, B. Gao, Z. Wang, *J. Electrochem. Soc*. **164** (2017) H126 (https://doi.org/10.1149/2.1381702jes)
28. A. O. Khudorozhkova, A. V. Isakov, A. A. Kataev, A. A. Redkin, Yu. P. Zaykov, *Russ. Metallurgy (Metally)* **2020** (2020) 918 (https://doi.org/10.1134/S0036029520080078)
29. Yu. P. Zaikov, A. A. Redkin, A. P. Apisarov, I. V. Korzun, N. P. Kulik, A. V. Isakov, A. A. Kataev, O. V. Chemezov, *J. Chem. Eng. Data* **58** (2013) 932 (https://doi.org/10.1021/je301195x)
30. S. Fletcher, C. S. Halliday, D. Gates, M. Westcott, T. Lwin, G. Nelson, *J. Electroanal. Chem.* **159** (1983) 267 (https://doi.org/10.1016/S0022-0728(83)80627-5)

31. D. Pletcher, R. Greff, R. Peat, L. M. Peter, J. Robinson, in *Instrumental Methods in Electrochemistry*, Woodhead, New Delhi, 2010, p. 210 (ISBN: 9781782420545).
32. V. A. Isaev, O. V. Grishenkova, A. V. Kosov, O. L. Semerikova, Y. P. Zaykov, *J. Solid State Electrochem*. **22** (2018) 2775 (https://doi.org/10.1007/s10008-018-3989-9)
33. B. R. Scharifker, G. J. Hills, *Electrochim. Acta* **28** (1983) 879 (https://doi.org/10.1016/0013-4686(83)85163-9)
34. V. A. Isaev, Yu. P. Zaykov, O. V. Grishenkova, A. V. Kosov, O. L. Semerikova, *J. Electrochem. Soc*. **166** (2019) D851 (https://doi.org/10.1149/2.1061915jes)
35. O. Díaz-Morales, J. Mostany, C. Borrás, B. R. Scharifker, *J. Solid State Electrochem*. **17** (2013) 345 (https://doi.org/10.1007/s10008-012-1881-6)
36. O. V. Grishenkova, A. V. Kosov, Yu. P. Zaikov, V. A. Isaev, *Russ. Metallurgy (Metally)* **2020** (2020) 914 (https://doi.org/10.1134/S0036029520080042)
37. I. G. Aksyanov, M. E. Kompan, I. V. Kul'kova, *Phys. Solid State* **52** (2010) 1850 (https://doi.org/10.1134/S1063783410090106)
38. N. A. Solopova, N. Dubrovinskaia, L. Dubrovinsky, *Appl. Phys. Lett.* **102** (2013) 121909 (http://dx.doi.org/10.1063/1.4798660)
39. Y.-J. Kim, M.-H. Kim, J.-H. Yang, J.-W. Park, *J. Korean Phys. Soc*. **49** (2006) 1196 (https://www.jkps.or.kr/journal/view.html?uid=7876&vmd=Full)
40. M. Becker, U. Gösele, A. Hofmann, S. Christiansen, *J. Appl. Phys*. **106** (2009) 074515 (https://doi.org/10.1063/1.3236571).